Battery-assisted and Photovoltaic-sourced Switched-inductor CMOS Harvesting Charger–Supply

Rajiv Damodaran Prabha, *Graduate Student Member, IEEE,* and Gabriel A. Rincón-Mora*, Fellow, IEEE*
Georgia Institute of Technology, Atlanta, Georgia 30332 U.S.A.
rajiv.damodaran@gatech.edu and Rincon-Mora@gatech.edu

***Abstract*—A challenge wireless microsensors and other microsystems face is short lifetime, because tiny batteries store little energy. Fortunately, the environment holds vast amounts of energy, and of available sources, like light, motion, temperature, and radiation, solar light produces the highest power density. Still, micro-scale photovoltaic (PV) cells harness a diminutive fraction of light and artificial lighting avails a small percentage of what solar light can, which means the PV cell needs assistance from a battery. Mixing PV and battery power to supply a microwatt system, however, requires a smart and low-loss circuit. For that, the battery-assisted pulse-width-modulated (PWM) buck–boost single-inductor 0.18-µm CMOS harvester–supply proposed and simulated here uses up to 100 µW from a PV cell to supply up to 1 mA and regulate 1 V within 25 mV at 10 – 80 kHz and with 77% – 89% efficiency.**

***Index Terms*—Harvester, photovoltaic (PV), microsystem, switched-inductor supply, switching converter, SIMO, SIMIMO**

I. Photovoltaic Microsystems

Wireless microsensors and other microsystems can add performance-enhancing and energy-saving intelligence to large infrastructures like factories and hospitals and unreachable places like the human body [1]. Small onboard batteries, however, deplete quickly, and lifetimes are, as a result, short. Fortunately, ambient energy is a vast source, and because solar power often overwhelms power derived from motion, temperature, and far-field radiation [2–3], photovoltaic (PV) cells generate considerable power.

Emerging microsensors, however, normally incorporate transmitters, receivers, analog–digital converters, sensor-interface circuits, and digital-signal processors that alone and combined draw substantial power. Although wireless transmission need not be continuous, high-activity periods can be long, and the power on-demand blocks, which operate continuously, demand often exceeds what mm-sized PV cells draw from artificial light [4]. In other words, assisting a tiny PV cell with a power source, be it a thin-film lithium-ion battery or a small super/ultra capacitor, is usually a necessity.

Supplying the 1-mW load in Fig. 1 from a 0 – 100-µW PV cell and a battery amounts to mixing PV power P_{PV} with battery power P_{PS}. The system therefore supplies load power P_O from P_{PV} and P_{PS} when lightly sourced and directs excess PV power P_{CHG} to the battery otherwise. Because a small PV cell captures only a fraction of the indoor light available, lightly sourced conditions are prevalent, so the system requires more energy across these periods T_{LS} than otherwise across T_{HS}. In other words, lightly sourced PV- and battery-to-load efficiencies η_{PV} and η_{PS} incorporate more energy than heavy-sourced PV-to-load and -battery efficiency η_{HS} because T_{LS} and P_{PS} are both considerably higher than T_{HS} and P_{PV}:

$$E_O + E_{CHG} = (\eta_{PV}P_{PV} + \eta_{PS}P_{PS})T_{LS} + \eta_{HS}P_{PV}T_{HS} \approx (\eta_{PV}P_{PV} + \eta_{PS}P_{PS})T_{LS} = P_{O.LS}T_{LS}. \quad (1)$$

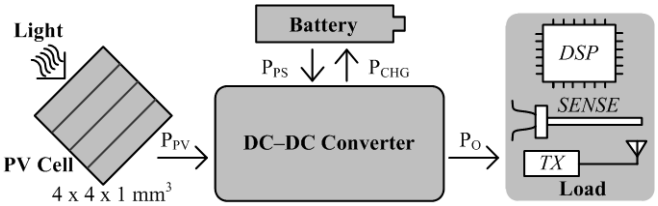

Fig. 1. Battery-assisted and photovoltaic-sourced wireless microsensor.

The aim of the harvester–supply described in Sections II and III is to derive up to 100-µW from a tiny PV cell exposed to artificial light and supply up to 1 mW to a 1-V load with as little assistance from the battery as possible. To ensure the cell is at its maximum-power point (MPP), the system controls the power it draws from the cell. Although not as often the case, the system also uses excess PV power during heavily sourced conditions to re-charge the battery, which the control circuit in Section IV ensures. Section V shows the harvesting and regulation performance of the system whose implications Section VI summarizes. The focus here is developing a circuit that can implement any of the MPP-tracking schemes in [5–8].

II. Battery-assisted Photovoltaic-sourced Supply

The switched inductor in Fig. 2 draws power from both a 0.25 – 0.4-V PV cell v_{PV} and a 1.8-V power source v_{PS} to supply a 1-V load with up to 1 mA. Relying on only one small off-chip power inductor L_X is important because off-chip inductors are bulky and their on-chip counterparts are poor, and altogether excluding the inductor drastically reduces power-conversion efficiency [9]. Input and output capacitors C_{IN} and C_O are also critical because they help keep L_X, PV, and load currents i_L, i_{PV}, and i_O from slewing v_{PV} away from its maximum-power point and output v_O away from its target V_{REF}.

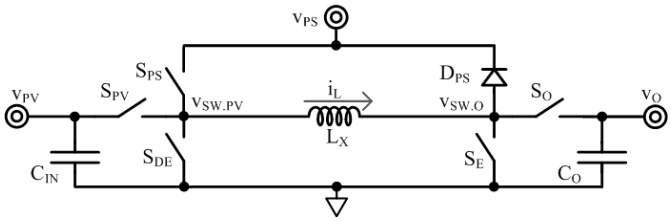

Fig. 2. Battery-assisted photovoltaic buck–buck charger–supply.

When lightly sourced, L_X draws and delivers energy to v_O first from v_{PV} and then from v_{PS}. For this, switches S_{PV} and S_E energize L_X from v_{PV} and S_{PV} and S_O subsequently drain L_X into v_O. After that, S_{PS} and S_O similarly energize L_X and S_{DE} and S_O de-energize L_X into v_O. Otherwise, when heavily sourced, L_X supplies P_O to the load from v_{PV} and charges v_{PS} with what remains of P_{PV}. As before, S_{PV} and S_E energize L_X and S_{PV} and S_O drain L_X into v_O, but unlike before, S_O opens when v_O receives P_O and i_L therefore charges switching node $v_{SW.O}$ until diode D_{PS} forward-biases and charges v_{PS} with i_L.

III. Harvesting Performance

The PV cell generates the most power when v_{PV} nears its optimal value of $V_{PV(OPT)}$, which means this system should adjust v_{PV} to $V_{PV(OPT)}$. Since the switching network induces a ripple voltage in v_{PV} that shifts the PV cell from its maximum-power point, v_{PV}'s ripple Δv_{PV} should be small. The circuit should also be able to modify and track v_{PV} to new targets to accommodate changes in light intensity and conditions [5].

Harvesting performance hinges on reducing power losses. Considering this, and tiny PV cells generate microwatts, ensuring L_X conducts continuously without reversing the direction of current amounts to keeping its rippling current Δi_L within a small window, which happens when L_X switches quickly. Charging and discharging the gates of power switches more often, however, requires more power, which is why L_X in Fig. 2 does not conduct continuously and switches slowly.

To ensure L_X derives sufficient PV power P_{PV} in one energizing (t_E) and de-energizing (t_{DE}) sequence, i_L rises to about 6 mA in Fig. 3. Transferring a larger energy packet E_{PV} in 1.6 µs draws sufficient P_{PV} from v_{PV} to keep v_{PV} from rising excessively over $V_{PV(OPT)}$ across the remaining 11.4 µs of the 13-µs period T_{SW}. Had E_{PV} been smaller and T_{SW} shorter, Δv_{PV} would have been less than 20 mV, except the power lost in switching more often negates the benefits of a smaller ripple.

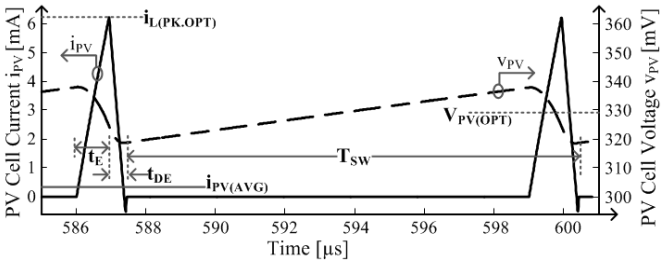

Fig. 3. Photovoltaic cell's voltage and current waveforms.

Output Power: The system ultimately consumes power, so v_O receives in P_O slightly less than what v_{PV} delivers with P_{PV}:

$$P_O = P_{PV} - P_{LOSS} = P_{PV} - P_R - P_G - P_Q . \quad (2)$$

Since v_O's ripple is small by design, the energy v_O receives when L_X drains (across t_{DE}) into v_O is the charge v_O collects from i_L at $v_{O(AVG)}$ across t_{DE}:

$$E_O = Q_L v_{O(AVG)} = 0.5 t_{DE} i_{L(PK)} v_{O(AVG)} , \quad (3)$$

where i_L falls to zero from its peak of $i_{L(PK)}$ when L_X de-energizes from v_{PV} to v_O, which means t_{DE} and P_O are

$$t_{DE} = \frac{L_X i_{L(PK)}}{v_{O(AVG)} - v_{PV(AVG)}} \quad (4)$$

and

$$P_O = \frac{E_O}{T_{SW}} = E_O f_{SW} = \frac{0.5 L_X i_{L(PK)}{}^2 v_{O(AVG)} f_{SW}}{v_{O(AVG)} - v_{PV(AVG)}} \propto i_{L(PK)}{}^2 f_{SW} . \quad (5)$$

In other words, frequency f_{SW} rises with P_O and falls quadratically with increasing values of peak current $i_{L(PK)}$:

$$f_{SW} \propto \frac{P_O}{i_{L(PK)}{}^2} . \quad (6)$$

Unfortunately, the system dissipates conduction power P_R across the switches, gate-drive power P_G to charge and discharge the gates of the switches, and quiescent power P_Q to control the switching sequence. Since the circuit supplies charge Q_C or $C_{EQ}\Delta v_C$ to charge capacitors C_{EQ} to Δv_C, for example, gate-drive energy E_G is a loss and P_G is

$$P_G = \frac{E_G}{T_{SW}} = Q_C \Delta v_C f_{SW} = C_{EQ} \Delta v_C{}^2 f_{SW} \propto \frac{P_O}{i_{L(PK)}{}^2} . \quad (6)$$

Parasitic resistances R_{EQ} in L_X, C_{IN}, and C_O and the switches [10], on the other hand, dissipate Ohmic power P_R or $i_{R(RMS)}{}^2 R_{EQ}$ when they conduct. Here, i_L's RMS current $i_{L(RMS)}$ across t_E and t_{DE} is $i_{L(PK)}/\sqrt{3}$ and $i_{L(RMS)}$ flows through R_{EQ} across conduction time t_C of the period T_{SW}:

$$P_R = i_{L(RMS)}{}^2 \left(\frac{t_C}{T_{SW}}\right) R_{EQ} = \left(\frac{i_{L(PK)}}{\sqrt{3}}\right)^2 R_{EQ} t_C f_{SW} \propto t_C P_O . \quad (7)$$

The controller also requires quiescent power P_Q to operate. Luckily, not all blocks need to function continuously, which means duty-cycling some of them is possible. As a result, duty-cycled components consume power $P_{Q(ON)}$ only when engaged, across t_{ON} of T_{SW}, so P_Q rises with t_{ON} and f_{SW}:

$$P_Q = P_{Q(DC)} + P_{Q(ON)} \left(\frac{t_{ON}}{T_{SW}}\right) = P_{Q(DC)} + P_{Q(ON)} t_{ON} f_{SW} \propto \frac{t_{ON} P_O}{i_{L(PK)}{}^2} . \quad (8)$$

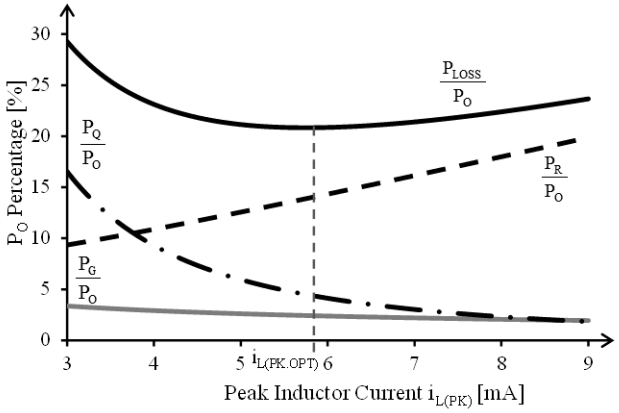

Fig. 4. Percentage of output power loss mechanisms represent.

Optimal Point: Because fixing L_X's energy packet via $i_{L(PK)}$ in Fig. 3 sets T_{SW} and *vice versa*, the design objective is to select the $i_{L(PK)}$–T_{SW} combination that reduces the percentage of P_{PV} lost to P_{LOSS} the most, or similarly, the percentage that P_{LOSS} is to P_O. Observing the P_O percentage of each loss mechanism reveals that, while P_G/P_O and P_Q/P_O fall almost quadratically with rising $i_{L(PK)}$ values, as Fig. 4 shows, P_R/P_O rises linearly

because raising $i_{L(PK)}$ increases L_X's conduction time t_E and t_{DE}, which extends the time that resistances in the circuit conduct i_L (i.e., raises t_C). So, since P_G and P_Q overwhelm P_R when $i_{L(PK)}$ is low and *vice versa* when $i_{L(PK)}$ is high, P_{LOSS}/P_O is lowest when $i_{L(PK)}$ is $i_{L(PK.OPT)}$, which sets f_{SW} to $f_{SW(OPT)}$.

IV. Control

The system must keep, as a harvester, v_{PV} near $V_{PV(OPT)}$ to ensure the PV cell is at its maximum-power point and, as a supply, v_O about V_{REF} to prevent power surges from affecting the load. For that, the harvester–supply in Fig. 5 controls v_{PV} and v_O by adjusting the power L_X draws from v_{PV} and v_{PS}, respectively. More specifically, energizing times $t_{PV.E}$ and $t_{PS.E}$ in Figs. 5 and 6 set how much energy L_X draws per cycle from v_{PV} and v_{PS}. So, when lightly sourced, which is the system's predominant state, the battery assists the PV cell; otherwise, when heavily sourced, excess PV power charges the battery.

Master clock T_{SW} starts and synchronizes the system to optimal switching frequency $f_{SW(OPT)}$. At $T_{SW(OPT)}$'s onset, M_{NPV} and M_{NE} energize L_X from v_{PV} to ground across $i_{E.PV}$–C_{PV}-defined delay $t_{PV.E}$. After that, v_{GE} falls to open M_{NE} and close M_{PO}, which de-energizes L_X into v_O. If lightly sourced, comparator CP_O trips to open M_{NPV} when L_X depletes: when the voltage that L_X's i_L produces across M_{PO} nears zero.

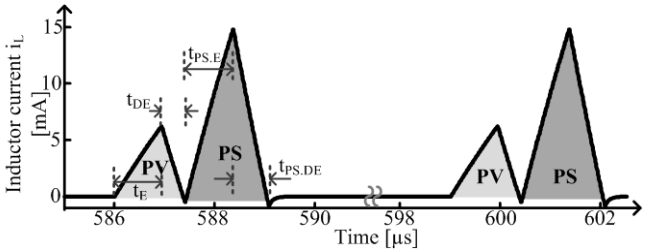

Fig. 6. Inductor-current waveforms.

At that point, CP_O also closes M_{PPS} and starts a ramp that comparator CP_{PWM} uses to pulse-width modulate (PWM) v_{PWM}, which sets the time ($t_{PS.E}$) that M_{PPS} energizes L_X from v_{PS} into v_O. So, after L_X depletes E_{PV} into v_O, CP_O prompts L_X to energize from v_{PS} and CP_{PWM} opens M_{PPS} and closes M_{NDE} after $t_{PS.E}$ to drain the energy L_X drew from v_{PS} into v_O. CP_O again detects when L_X depletes to open M_{PO} and M_{NDE} and close M_{NR}, the latter of which consumes remnant energy left in L_X that would otherwise cause oscillations. The system does not energize L_X again until $T_{SW(OPT)}$ rises again.

When heavily sourced, however, L_X does not fully drain E_{PV} into v_O, which means CP_O does not prompt L_X to draw assistance from v_{PS}. Instead, comparator CP_{HS} opens M_{PO} when v_O rises 40 mV above V_{REF}, allowing remnant current in L_X to raise $v_{SW.O}$ until diode D_{PS} forward-biases to v_{PS}. The battery then charges until L_X drains, when i_L falls to zero. As before, the system re-starts the cycle when $T_{SW(OPT)}$ rises.

PWM Loop: Error amplifier EA_O compares v_O against V_{REF}, and together with CP_{PWM}, pulse-width modulates v_{PWM} to control $t_{PS.E}$: how long L_X energizes from v_{PS}. In particular, CP_{PWM} compares EA_O's output v_{EA} to a ramp, so v_{PWM} is high when the ramp is below v_{EA} and low otherwise, which means v_{PWM}'s (low-state) pulse width $t_{PS.E}$ increases with v_{EA}. This way, with negative feedback, EA_O raises v_{EA} (and $t_{PS.E}$) when v_O drops below V_{REF}, which prompts L_X to draw and supply more battery energy to the load.

As in typical PWM loops, EA_O and the ramp set the low-frequency gain of the loop [11–13]. Since L_X operates in discontinuous-conduction mode (DCM), L_X and C_O introduce only one output pole p_O at $1/2\pi R_O C_O$. EA_O's output R_{EA} also introduces another pole p_{EA}, which is why R_F current-limits C_F to insert a zero at $1/2\pi R_F C_F$ with which to offset a pole. R_F and C_F also pull p_{EA} to lower frequency: to $1/2\pi(R_{EA} + R_F)C_F$, to ensure p_{EA} is dominant and allow the loop gain to reach 0 dB with 90^O of phase margin.

V. Simulated Performance

Implementation: The 0.18-µm CMOS integrated circuit (IC) and 47-µH–5.6-Ω L_X in Fig. 5 derived power from a 4 × 4 × 1-mm^3 OSRAM PV cell when exposed to indoor lighting conditions. To reduce gate-drive losses P_G, channel lengths are short at 0.18 µm. Since increasing channel widths raise P_G and reduce Ohmic losses P_R, the selected widths balance P_G and P_R [10] at mean conditions, when PV power is 50 µW and the load demands 0.5 mW. M_{PO}'s resistance is sufficiently

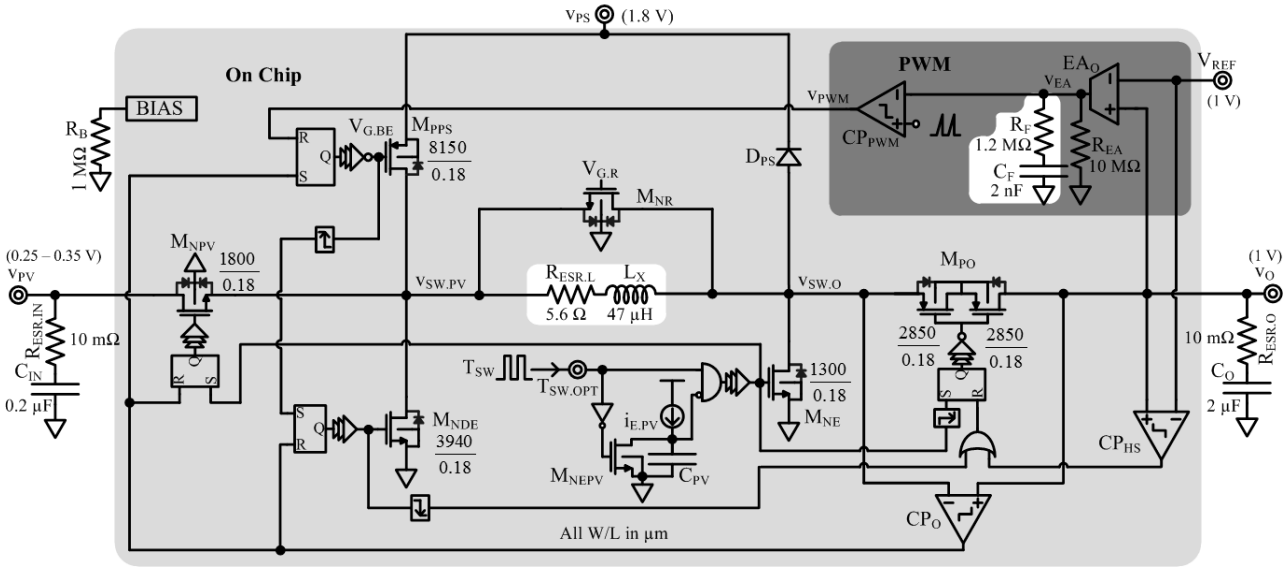

Fig. 5. Battery-assisted photovoltaic harvester–supply system.

high to ensure CP_O's 10-mV offset only affects small i_L values. In addition to operating in sub-threshold, $t_{PV.E}$, CP_O, EA_O, and CP_{PWM} and its ramp function only when needed, in sequence after $T_{SW(OPT)}$.

Regulation: The system regulates v_O to 1 V with 5 and 24 mV of ripple when loaded with 100 µW and 1 mW, respectively, as the simulated results of Fig. 7 verify. When load suddenly rises from 100 µW to 1 mW and switching frequency f_{SW} is at 10 kHz, which happens when PV power is 10 µW, v_O droops 85 mV before the system recovers. The response time shortens when P_{PV} rises to 100 µW, at which point f_{SW} is 80 kHz.

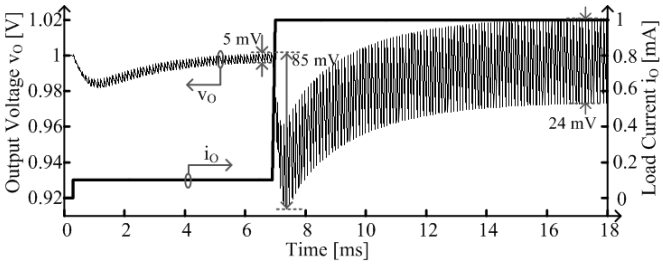

Fig. 7. Simulated load-dump response and steady-state waveforms.

When lightly loaded, the system regulates v_O to 1 V and steers excess P_{PV} to the battery. As Fig. 8 shows, the system consumes 32 µW of the incoming 107 µW to supply 50 µW to the load and 25 µW to a 1-µF power source C_{BAT}. As a result, the harvester charged C_{BAT} 1.6 mV in 100 µs with 70% power-conversion efficiency.

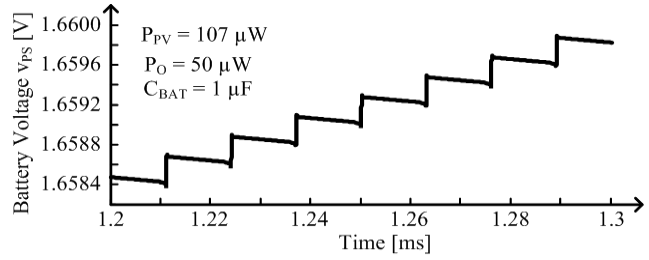

Fig. 8. Simulated battery-charge profile when heavily sourced.

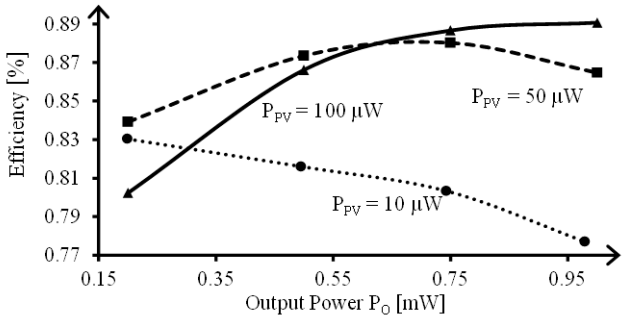

Fig. 9. Simulated conversion efficiency when lightly sourced.

Efficiency: When lightly sourced, which is the predominant state for the system, efficiency $\eta_{S(LS)}$ in Fig. 9 illustrates how much PV power P_{PV} and battery power P_{PS} reach the load as P_O:

$$\eta_{S(LS)} \equiv \frac{P_O}{P_{PV} + P_{PS}} . \quad (9)$$

As designed, losses balance when P_{PV} is 50 µW (at 50 kHz) and P_O is 0.5 mW, so $\eta_{S(LS)}$ in Fig. 9 peaks at 88%. When P_{PV} is 100 µW, however, $\eta_{S(LS)}$ steadily rises with P_O until peaking at 89% because at 80 kHz, as in typical microwatt converters [14–15], gate-drive losses dominate over the entire range of P_O. On the other hand, when P_{PV} is 10 µW (at 10 kHz), $\eta_{S(LS)}$ rises because conduction losses dominate across P_O's range.

VI. Conclusions

The battery-assisted single-inductor harvester–supply presented and simulated here draws up to 100 µW from a 4 × 4 × 1-mm^3 photovoltaic (PV) cell to supply up to 1 mW with 77% – 89% efficiency and regulate 1 V within 25 mV in steady state and 85 mV in response to sudden 900-µA load dumps. In addition to operating in sub-threshold and duty-cycling subsystems to save energy, the converter operates the inductor discontinuously at switching frequencies that minimize losses for mid-range power levels. Drawing power from chip-sized PV cells illuminated indoors and enlisting assistance from a battery to supply milliwatt loads is important because miniaturized indoor military, consumer, industrial, and medical applications in this power range are vast.

References

[1] G. Chen *et al.*, "A cubic-millimeter energy-autonomous wireless intraocular pressure monitor," *Int. Solid-State Circuits Conference*, pp. 310-312, 2011.

[2] R.D. Prabha *et al.*, "Harvesting circuits for miniaturized photovoltaic cells," *IEEE Int. Symp. on Circuits and Systems*, pp. 309-312, May 2011.

[3] E.O. Torres and G.A. Rincón-Mora "Long-lasting, self-sustaining, and energy-harvesting system-in-package (SiP) wireless micro-sensor solution", *Int. Conf. on Energy, Environment, and Disasters*, pp. 1-33 , Jul. 2005.

[4] G. Chen *et al.*, "Circuit design advances for wireless sensing applications, " Proc. IEEE, vol. 98, no. 11, pp. 1808–1827, Nov. 2010.

[5] T. Esram *et al.,* "Comparison of Photovoltaic Array Maximum Power Point Tracking Techniques," *IEEE Trans. on Energy Conversion*, vol. 22, no. 2, pp. 439-449, June 2007.

[6] H. Shao *et al.*, "An inductor-less micro solar power management system design for energy harvesting applications," *IEEE Int. Symp. on Circuits and Systems*, pp. 1353-1356, 2007.

[7] Q. Yifeng *et al.*, "5µW-to-10mW input power range inductive boost converter for indoor photovoltaic energy harvesting with integrated maximum power point tracking algorithm," *Int. Solid-State Circuits Conference*, pp.118-120, Feb. 2011.

[8] D. Brunelli *et al.,* "Design of a Solar-Harvesting Circuit for Batteryless Embedded Systems," *IEEE Trans. on Circuits and Systems I*, vol. 56, no. 11, pp. 2519-2528, Nov. 2009.

[9] M. Chen and G.A. Rincon-Mora, "Single Inductor, Multiple Input, Multiple Output (SIMIMO) Power Mixer-Charger-Supply System," *Int. Symp.on Low Power Electronics and Design*, pp. 310-315, 2007.

[10] S. Kim and G.A. Rincon-Mora, "Achieving High Efficiency under Micro-Watt Loads with Switching Buck DC-DC Converters, " *Journal of Low-Power Electronics*, vol. 5, no. 2, Aug. 2009.

[11] G.A. Rincon-Mora, *Power IC Design*, Raleigh: Lulu, 2009.

[12] A. Pressman, *Switching Power Supply Design*, New York: McGraw-Hill, 1991.

[13] R. Erickson and D. Maksimovic, *Fundamentals of Power Electronics, 2nd Ed.*, New York: Springer Science & Business Media, LLC, 2001.

[14] H. Shao *et al.*, "A single inductor dualinput dual output DC–DC converter with hybrid supplies for solarenergy harvesting applications," *Int. Symp. on LowPower Electronics and Design*, pp. 69–74, 2009.

[15] H. Shao *et al.*, "A single inductor DIDO DC-DC converter for solar energy harvesting applications using band-band control," *VLSI System on Chip Conference*, pp.167-172, Sep. 2010.